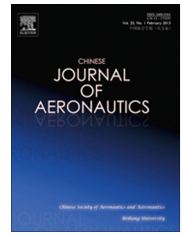




Chinese Society of Aeronautics and Astronautics
& Beihang University

Chinese Journal of Aeronautics

cja@buaa.edu.cn
www.sciencedirect.com



Robust adaptive fault-tolerant control of a tandem coaxial ducted fan aircraft with actuator saturation

Xiaoliang WANG^{a,*}, Changle XIANG^a, Homayoun NAJJARAN^b, Bin XU^a

^a Vehicle Research Center, School of Mechanical Engineering, Beijing Institute of Technology, Beijing 100081, China

^b Okanagan School of Engineering, The University of British Columbia, Kelowna V1V 1V7, Canada

Received 27 April 2017; revised 9 June 2017; accepted 30 September 2017

Available online 27 March 2018

KEYWORDS

Comprehensive controllability;
Ducted fan aircraft;
Fault-tolerant;
Input saturation;
Robust adaptive control

Abstract This paper is concerned with the robust adaptive fault-tolerant control of a tandem coaxial ducted fan aircraft under system uncertainty, mismatched disturbance, and actuator saturation. For the proposed aircraft, comprehensive controllability analysis is performed to evaluate the controllability of each state as well as the margin to reject mismatched disturbance without any knowledge of the controller. Mismatched disturbance attenuation is ensured through a structured H-infinity controller tuned by a non-smooth optimization algorithm. Embedded with the H-infinity controller, an adaptive control law is proposed in order to mitigate matched system uncertainty and actuator fault. Input saturation is also considered by the modified reference model. Numerical simulation of the novel ducted fan aircraft is provided to illustrate the effectiveness of the proposed method. The simulation results reveal that the proposed adaptive controller achieves better transient response and more robust performance than classic Model Reference Adaptive Control (MRAC) method, even with serious actuator saturation.

© 2018 Chinese Society of Aeronautics and Astronautics. Production and hosting by Elsevier Ltd. This is an open access article under the CC BY-NC-ND license (<http://creativecommons.org/licenses/by-nc-nd/4.0/>).

1. Introduction

The ducted fan aircraft, as a novel aircraft design, is driving evident research interest in academic and industrial communities. Since 1990s, many countries have started research in this field one after another, and have developed different ducted

aerial aircrafts.¹ Compared with traditional flight aircrafts, the ducted fan aircraft has special characteristics that enable it to complete various applications on areas that are unknown, dangerous, and inaccessible to traditional aircrafts. The protected rotor blades of the ducted fan aircrafts are compatible with the environments potentially cluttered with obstacles. Moreover, a ducted fan produces more thrust than an open rotor at the same blade size. These features also ensure a markedly compact body design with strong mobility, low noise, and high efficiency.^{2,3}

In Beijing Institute of Technology (BIT), several prototypes of the ducted fan aircraft have been designed for research on modelling, system identification and flight control algorithms.^{2,4,5} The design iterations of the ducted fan aircraft in

* Corresponding author.

E-mail address: wangxiaoliang1992@gmail.com (X. WANG).

Peer review under responsibility of Editorial Committee of CJA.



Production and hosting by Elsevier

BIT is shown in Fig. 1. However, for the first two prototypes, they have proved to reveal poor stability and controllability due to structural coupling.⁴ Under this context, as shown in Fig. 2, the latest prototype adopts two ducts with coaxial rotors and control vanes. In order to illustrate the features of the new design, the moment generation mechanism of these prototypes is given in Table 1. For the latest model, pitch and yaw moment are generated by changing the speed of the four rotors. To be specific, roll moment is regulated by the control vanes. Compared to the previous ones, this newly adopted structure is able to provide more control moments with the same size duct, especially in roll direction. On that case, the new aircraft is expected to achieve better decoupling features and controllability.

In order to achieve various types of civil and military applications, the novel ducted fan aircraft must have the strong ability for trajectory tracking independent of the atmospheric conditions. A number of approaches to flight control of novel ducted fan aircraft and other UAVs have been applied to a variety of problems. For example, as a classic control method, PID controller is used by Sheng and Sun,⁶ but it is not robust to noise and disturbance, and therefore fails to ensure performance for full envelop flight. Dynamic inversion control and sliding mode control are also presented.^{7,8} Although these control algorithms are able to reject external disturbance and achieve good control performance in simulations, they rely on known and accurate system model. Neural Network (NN) techniques also have been widely employed for robots in literatures. He et al.⁹ applies an NN controller to suppress the vibration of a flexible robotic manipulator system with input deadzone. Although input deadzone and unknown dynamics can be approximated, the method does not consider large disturbance and is just validated by Single Input Single Output (SISO) system. Adaptive NN¹⁰ and adaptive fuzzy NN¹¹ are used to identify system uncertainties and disturbance for a constrained robot. However, their methods are of great complexity and difficult to utilized in practical engineering. In consideration of model errors, H-infinity control and adaptive control are widely adopted. Successive two-loop control architecture⁵ is employed and control gains are well tuned by Non-smooth optimization method. This control structure ensures robust stabilization, but transient tracking performance drops when large uncertainty are included. Indirect adaptive control schemes⁶ and adaptive gain scheduling algorithm¹² are respectively adopted to deal with parametric uncertainty. These adaptive control methods guaranteed small tracking error and the convergence of adjustable parameters.

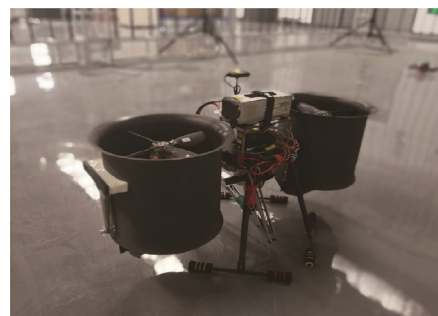


Fig. 2 Novel ducted fan aircraft from BIT (third generation).

Table 1 Moments generation mechanism of ducted fan aircrafts in BIT.

Control moment	1st prototype	2nd prototype	3rd prototype
Roll	Actuation of control vanes	Speed difference of auxiliary ducted fans	Actuation of control vanes
Pitch	Speed difference of main rotors	Speed difference of main rotors	Speed difference of coaxial main rotors
Yaw	Actuation of control vanes	Tilting auxiliary ducted fans	Speed difference of coaxial main rotors

However, the dynamics is over simplified and dynamic couplings is not considered. Standard Model Reference Adaptive Control (MRAC) framework¹³ is proposed to cope with system uncertainty and also guarantees that the tracking error decreases asymptotically to zero. Unfortunately, the previous research does not take mismatched disturbance into consideration.

On the other hand, an important problem encountered in practice is actuator saturation because it is frequently one of the main sources of instability, degradation of system performance, and parasitic equilibrium points of a control system.¹⁴ Some solutions have been provided to handle input constraint for flight control system. Based on structured H-infinity optimization, an anti-windup compensator¹⁵ is designed to preserve stability and maintain the performance level under input saturations. Guaranteed transient performance based attitude control with input saturation is also proposed using

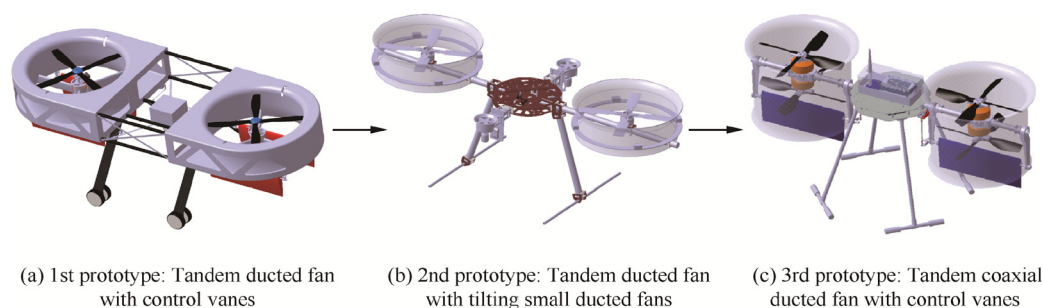


Fig. 1 Design iterations of ducted fan aircrafts in BIT.

the backstepping method.¹⁶ Nevertheless, these methods cannot ensure control performance in the presence of large mismatched disturbance and system uncertainty. Auxiliary system^{17,18} that is embedded to Lyapunov function is also adopted to deal with input saturation. Nevertheless, the effect of the auxiliary system parameters on system performance is implicit, which could result in a very conservative design. Zhang et al.¹⁹ adopts robust Model Predictive Control (MPC) algorithms that transforms the design problem into a minimization problem of a worst-case performance index with respect to model uncertainty. However, the designed controller is too conservative to achieve fast tracking and high bandwidth.

In addition to flight control aspects, property of controllability that relates to the mechanical design is equally important in practice. Skogestad and Postlethwaite²⁰ have proved that input–output controllability is independent of controller. This property, related to its mechanical structure of the real plant, is able to show inherent limitations on system control and the ability to reject external disturbance. Thus we will start with a comprehensive controllability analysis to provide insightful suggestions for mechanical design. In this study, robust adaptive fault-tolerant tracking control is presented for the novel ducted fan aircraft. The proposed method benefits techniques of H-infinity control and adaptive control. Considering mismatched disturbance, the baseline controller tuning is completed by non-smooth optimization algorithm²¹ in structured H-infinity synthesis, which provides reference dynamics for adaptive control. Motivated by the classic MRAC algorithm^{22–24}, the adaptive control augmentation is then applied to recover the desired performance in the presence of system uncertainty, mismatched disturbance and actuator fault. Further, the reference model modification in consideration of transient response and actuator saturation is then performed to improve robustness and tracking accuracy.

The remaining part of the paper is organized as follows: system model and comprehensive controllability analysis are first presented in Section 2; Robust H-infinity synthesis for baseline controller is proposed in Section 3; Section 4 details the design of augmented adaptive control law; and finally, we draw concluding remarks in Section 5.

2. System model and comprehensive controllability analysis

2.1. Model description

Modelling of ducted fan dynamics is one the popular topics in the literature of unmanned aircrafts. Based on aerodynamics of open rotors, Johnson and Turbe²⁵ proposes a modified momentum model by an inflow theory. In some researches^{4,26}, duct effect is simply represented by inflow deflection and thrust augmentation due to the suction flow of the lip. However, regarding duct with coaxial rotors, the dynamics is much more complicated than duct with single rotor.³ Based on our results of Computational Fluid Dynamics (CFD) that is shown in Fig. 3, the duct generates almost half of the total thrust, and the lower rotor produces more lift than the upper counterpart, which challenges the conclusions by Ohanian¹ and Jang et al.²⁷ Therefore, it is very difficult to capture complete dynamics of duct fan with coaxial rotors by mechanism modeling. In this work, instead of complex nonlinear model with a number of

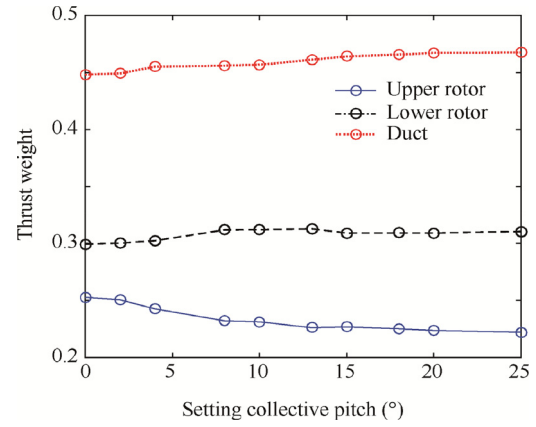


Fig. 3 CFD results for proposed novel ducted fan aircraft.

unknown parameters, we adopt a simple control-oriented model.

Thus, system state vector $\mathbf{x}_p \in \mathbf{R}^{n_p}$ and control input $\mathbf{u} \in \mathbf{R}^n$ are defined as

$$\begin{cases} \mathbf{x}_p = [U, V, W, p, q, r, \phi, \theta, \psi]^T \\ \mathbf{u} = [u_{col}, u_{lat}, u_{lon}, u_{ped}]^T \end{cases} \quad (1)$$

where $[U, V, W]^T$ represents body-axis velocity, $[p, q, r]^T$ and $[\phi, \theta, \psi]^T$ are respectively Euler angular rate and angle. \mathbf{u} is input vector and each of its components is normalized to $[-1, 1]$. The normalization of input vector is very important. First, the normalized input helps the elements of control matrix to keep at a proper scale, and avoid control matrix to be ill conditioned. Second, this normalization also ensures similar scale for the components of transfer function matrix of the closed-loop system, which is necessary to H-infinity framework on system tuning.

Linearized at trimming points, the uncertain system model²² is

$$\begin{cases} \dot{\mathbf{x}}_p = \mathbf{A}_p \mathbf{x}_p + \mathbf{B}_p \mathbf{A}(\mathbf{u} + \mathbf{\Theta}^T \mathbf{\Phi}(\mathbf{x}_p)) + \boldsymbol{\xi}(t) \\ \boldsymbol{\xi}(t) = \mathbf{B}_d \mathbf{w}_d(t) \end{cases} \quad (2)$$

where \mathbf{A}_p and \mathbf{B}_p are respectively system state matrix and control matrix. The matched system uncertainty is represented by $\mathbf{\Theta}^T \mathbf{\Phi}(\mathbf{x}_p)$. $\mathbf{\Theta}$ is real matrix, and $\mathbf{\Phi}(\mathbf{x}_p)$ is the known N-dimensional regressor vector whose components are locally Lipschitz-continuous functions of \mathbf{x}_p . This matched uncertainty is introduced to consider unmodelled dynamics and model errors. \mathbf{A} denotes actuator fault that could be uncertain control gains or incorrectly estimated the system control effectiveness.¹³

The system is also under a uniformly bounded time-dependent disturbance $\boldsymbol{\xi}_{\max}$, which is mismatched disturbance,²²

$$\|\boldsymbol{\xi}(t)\| = \|\mathbf{B}_d \mathbf{w}_d(t)\| \leq \boldsymbol{\xi}_{\max} \quad (3)$$

where $\mathbf{w}_d(t)$ is related to unknown moments and forces, $\boldsymbol{\xi}_{\max}$ is the bound of mismatched disturbance, and $\|\cdot\|$ denotes H-infinity norm of vector. In this way, the disturbance vector and the parameter matrix are as follows

$$\begin{cases} \mathbf{w}_d = [d_U, d_V, d_W, d_p, d_q, d_r]^T \\ \mathbf{B}_d = \begin{bmatrix} \mathbf{I}_{6 \times 6} \\ \mathbf{0}_{3 \times 6} \end{bmatrix} \end{cases} \quad (4)$$

where $d_U, d_V, d_w, d_p, d_q, d_r$ are respectively disturbance for state U, V, W, p, q and r .

In order to obtain nominal system matrix A_p and B_p , closed-loop flight tests have been performed in hovering condition. We followed standard steps for system identification,^{28,29} which will not be detailed in this paper. The identification results are as follows

$$A_p = \begin{bmatrix} -0.0876 & 0 & 0 & 0 & 0 & 0 & 0 & -9.8010 & 0 \\ 0 & -0.0876 & 0 & 0 & 0 & 0 & 9.8010 & 0 & 0 \\ -0.1178 & -0.1172 & -1.0415 & -0.0012 & -0.0209 & -0.0509 & 0 & 0 & 0 \\ 0 & -0.6801 & 0 & 0 & 0 & 0 & 0 & 0 & 0 \\ 0.0940 & 0 & 0 & 0 & -1.0699 & 0.0132 & 0 & 0 & 0 \\ 0 & 0 & 0 & 0 & -0.0122 & 0 & 0 & 0 & 0 \\ 0 & 0 & 0 & 1 & 0 & 0 & 0 & 0 & 0 \\ 0 & 0 & 0 & 0 & 1 & 0 & 0 & 0 & 0 \\ 0 & 0 & 0 & 0 & 0 & 1 & 0 & 0 & 0 \end{bmatrix}, B_p = \begin{bmatrix} 0 & 0 & 0 & 0 \\ 0.0121 & -0.1125 & 0 & 0 \\ -20.9312 & 0 & 0.0547 & -0.0015 \\ 0 & 8.3494 & 0 & 0.0620 \\ 0 & -0.0025 & 10.0876 & -0.0281 \\ 0 & 0.0216 & 0.3337 & 3.3981 \\ 0 & 0 & 0 & 0 \\ 0 & 0 & 0 & 0 \\ 0 & 0 & 0 & 0 \end{bmatrix}$$

2.2. Comprehensive controllability analysis with mismatched uncertainty

Controllability is an important property of a control system and plays a crucial role in many control problems, in terms of evaluation of system controllability, a classic way is to compute the controllability matrix³⁰

$$T_c = [B_p, A_p B_p, \dots, A_p^{n_p-1} B_p] \quad (5)$$

It is easy to verify that our nominal system (A_p, B_p) is controllable. Nevertheless, the system that achieves classic controllability often disregards the quality of the response between and after these states, and the magnitude of required inputs may be excessive.⁵ In that case, motivated by Singular Value Decomposition (SVD),³¹ we propose an alternative solution that enables to quantify actual ease of system control in frequency-domain, which is called comprehensive controllability analysis.

Since we focus on nominal system with external disturbance (mismatched disturbance), matched system uncertainty and actuator fault are ignored. In this way, system model is then released to

$$\begin{cases} \dot{x}_p = A_p x_p + B_p u + \xi(t) \\ \xi(t) = B_d w_d(t) \end{cases} \quad (6)$$

We first factorize the nominal system into a standard SVD,

$$G = U_m S V_m^H \quad (7)$$

where U_m and V_m are respectively output matrix and input matrix, S is singular value matrix, $(\cdot)^H$ denotes conjugate transpose. These corresponding matrices are given as follows

$$\begin{cases} S = \begin{bmatrix} \text{diag}(\sigma_1, \sigma_2, \dots, \sigma_n) \\ 0_{(n_p-n) \times n} \end{bmatrix} \\ U_m = [U_1, U_2, \dots, U_n] \\ V_m = [V_1, V_2, \dots, V_n] \end{cases} \quad (8)$$

where $\text{diag}(\cdot)$ denotes diagnose matrix, and σ denotes singular value.

Then comprehensive controllability gain is proposed as follows:

System input u is rewritten as the sum of bases for each control channel,

$$\begin{cases} u = \sum_{i=1}^4 \beta_i u_i \\ u_1 = [1, 0, 0, 0]^T \\ u_2 = [0, 1, 0, 0]^T \\ u_3 = [0, 0, 1, 0]^T \\ u_4 = [0, 0, 0, 1]^T \end{cases} \quad (9)$$

where β_i is the coefficient of components of the input vector u , and u_i is the base for each control channel. For the sake of input normalization, we have

$$|\beta_i| \leq 1 \quad (10)$$

The comprehensive controllability gain is defined as

$$g_u(\omega) = \max \|Gu\|, \quad u = \sum_{i=1}^4 \beta_i u_i \quad (11)$$

where ω is frequency.

Through SVD, system input u is rotated by input matrix V_m , and the rotated input u^* can be represented by the new bases

$$u^* = V_m u = \sum_{i=1}^4 \theta_i V_i \quad |\theta_i| \leq 1 \quad (12)$$

where θ_i is denotes the coefficient of components of rotated input vector u^* and V_m is output matrix for SVD.

According to property of matrix norm, since the input matrix $\|V_m\| = 1$, we have

$$\|Gu\|_{\max} = \|G \cdot (V_m u)\|_{\max} = \|Gu^*\|_{\max} \quad (13)$$

where $\|\cdot\|_{\max}$ denotes maximum H-infinity.

An essential property of SVD is

$$GV_i = \sigma_i U_i \quad i = 1, 2, 3, 4 \quad (14)$$

where U_i and V_i are respectively components of output matrix U_m and input matrix V_m in Eq. (8).

In this way, the gain is deduced by

$$\begin{aligned}
g_u(\omega) &= \|Gu\|_{\max} = \|Gu^*\|_{\max} = \left\| \sum_{i=1}^4 \theta_i G V_i \right\|_{\max} \\
&= \left\| \sum_{i=1}^4 \theta_i \sigma_i U_i \right\|_{\max} = \left\| \sqrt{\left(\sum_{i=1}^4 \theta_i \sigma_i U_i \right)^2} \right\|_{\max} \\
&= \left\| \sqrt{\left(\sum_{i=1}^4 \theta_i^2 \sigma_i^2 U_i^2 \right) + \sum_{i=1, j=1, i \neq j}^4 \theta_i \theta_j \sigma_i \sigma_j U_i U_j} \right\|_{\max} \quad (15)
\end{aligned}$$

Since U_m is orthogonal matrix, then

$$U_i U_j = 0 \quad i \neq j \quad (16)$$

Therefore, the comprehensive controllability gain is calculated by

$$g_u(\omega) = \left\| \sqrt{\sum_{i=1}^4 \theta_i^2 \sigma_i^2 U_i^2} \right\|_{\max} = \sum_{i=1}^4 \sigma_i \|U_i\| \quad (17)$$

It is shown in Fig. 4 that comprehensive controllability gain of most states in low frequency are more than 1, indicating that controllability for those states is excellent. Unfortunately, roll channel is difficult to control due to the low controllability gain in roll angle and roll angular rate, which also means that robust stability margin of roll channel is fundamentally small for closed-loop system.

Eq. (17) provides the maximum gain from system input to all states in frequency domain. Similarly, it is easy to calculate the maximum gain from mismatched disturbance to system output, and the disturbance system is defined by

$$G_d = \begin{bmatrix} A_p & C_d \\ B_d & 0 \end{bmatrix} \quad (18)$$

Then we get a solution to estimate the maximum tolerance of mismatched disturbance for the linear model. The gain generated by disturbance should be compensated by system input, so we have the following constraints

$$\begin{cases} k_m = \max\{k\} \\ g_u(\omega) \geq k g_d(\omega) \\ \omega \in (0, \omega_0) \\ \|w_d(i)\| \leq 1, \quad i = 1, 2, \dots, 6 \end{cases} \quad (19)$$

where $g_d(\omega)$ denotes comprehensive controllability gain for mismatched disturbance and k_m denotes maximum disturbance tolerance. Note that we just focus on states that follow the reference command, i.e. U , V , W , and ψ .

The reason why the inner-loop states (ϕ , θ , p , q , and r) are removed is that these states will deviate from trimming to compensate disturbance. In terms of our nominal system, the calculated maximum disturbance tolerance is $k_m = 2.1055$, indicating that the nominal system is able to attenuate disturbance that is less than 2.1055 times as unit disturbance in each direction. Corresponding controllability gains are plotted in Fig. 5. It is shown that the disturbance makes the greatest influence on yaw angle ψ in low frequency, because yaw channel have already reached the maximum tolerant magnitude rather than other states. In other words, the system has to make large control effort in yaw channel (u_{ped}) to deal with disturbance. Hence, there is low margin for disturbance rejection in yaw channel for our new designed aircraft.

3. Robust H-infinity synthesis for baseline controller

The control goal of interest of ducted fan aircraft is to track and execute reference commands provided by a pilot, a guidance logic, or an autonomous mission planner. It turns out that controllers that combine robust and adaptive components work very well in practical applications by maintaining closed-loop stability and enforcing robustness against uncertainty.²² To obtain a clear understanding of the controlled system, the proposed control structure diagram is given in Fig. 6. This control framework embeds robust baseline controller and its adaptive augmentation. The reference model is used to capture desired dynamics achieved by baseline controller for nominal system. The adaptive augmentation is applied to recover the desired performance in the presence of uncertainty and actuator fault. Note that input saturation is also considered to make the closed-loop system more robust and practical.

In this work, we will present rigorous steps for robust adaptive fault tolerant control of our novel ducted fan aircraft. This control problem is divided into two sub-problems: robust baseline control design and the adaptive augmentation, each with its own design objective. The first step, i.e. robust baseline control, is presented in this section.

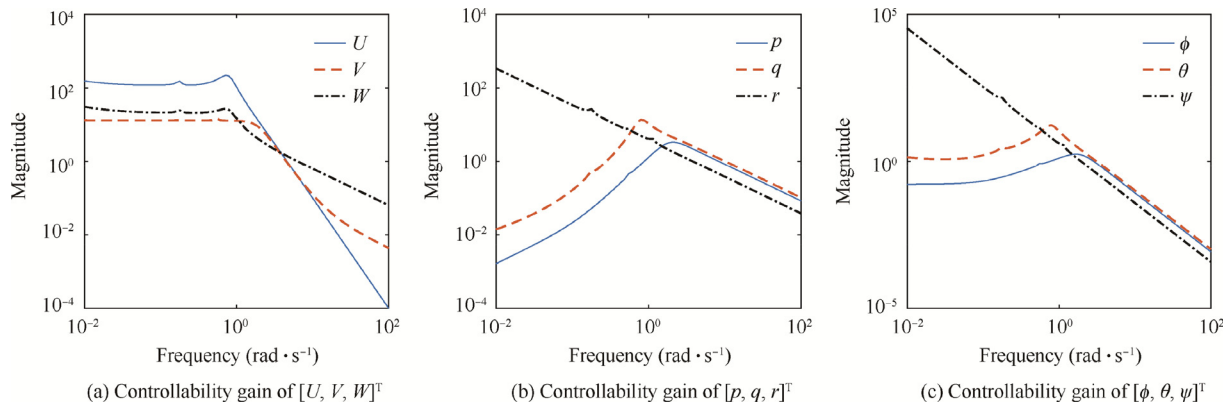


Fig. 4 Comprehensive controllability gain of each state for nominal system.

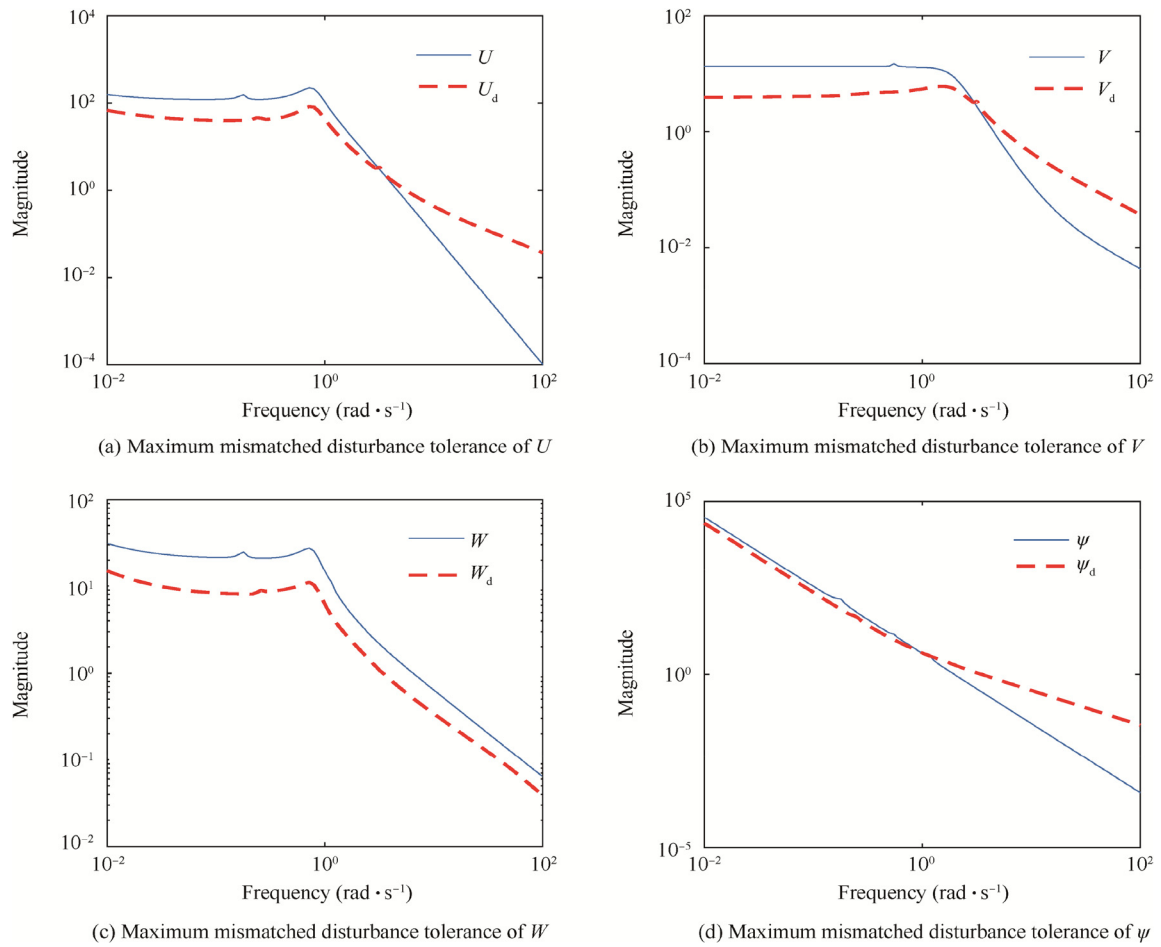


Fig. 5 Comprehensive controllability gain for nominal system with maximum tolerance of mismatched disturbance.

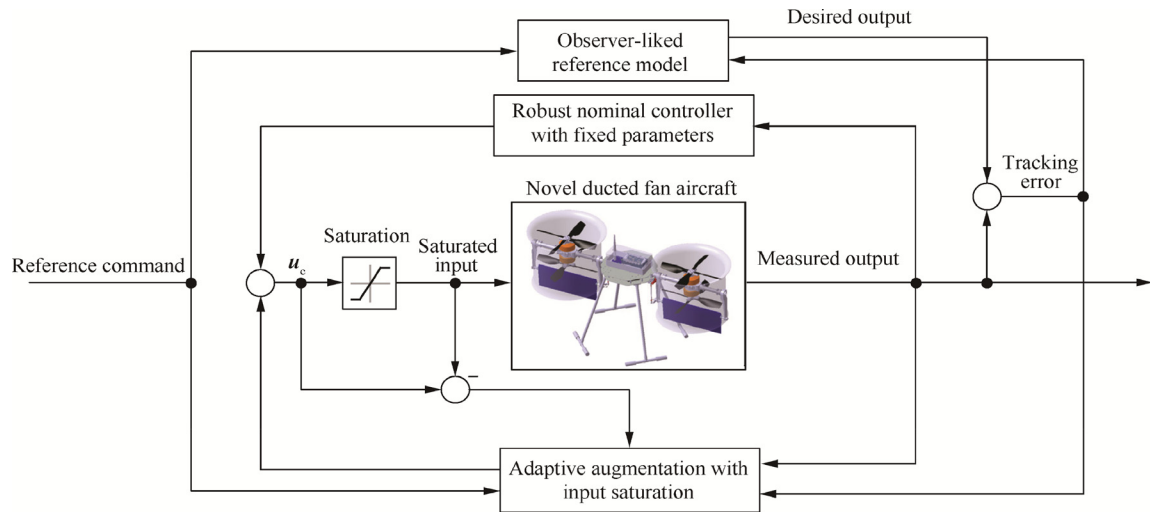


Fig. 6 Robust adaptive flight control configuration.

3.1. Structured baseline controller design via Non-smooth optimization

As shown in Fig. 6, the reference model represents the baseline closed-loop dynamics that would be achieved under the base-

line controller and without any uncertainty and actuator fault.²² Then this desired dynamics is expected to be followed by actual response through the adaptive control law when uncertainty and actuator fault are included. Therefore, it is necessary to find robust control structure for baseline control

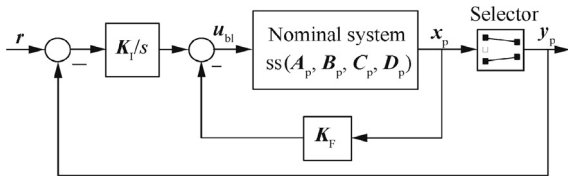


Fig. 7 Baseline control configuration.

that asymptotically rejects mismatched disturbance and track reference commands accurately with constrained control input. The adopted baseline control configuration is plotted in Fig. 7. The inner loop, in degrees for static state feedback control, is responsible for stabilization and decoupling, and the outer loop with integral feedback connections is applied to provide the desired command-tracking performance.

The system output tracking error is

$$e_y = y - r = C_p x_p - r \quad (20)$$

where $r = [U_{\text{ref}}, V_{\text{ref}}, W_{\text{ref}}, \psi_{\text{ref}}]^T$ is reference command, and $y = [U, V, W, \psi]^T$ is system output.

Then the system states x_p is augmented with integrated output tracking error

$$\begin{cases} x_a = [e_{yI}, x_p^T]^T \\ e_{yI}(s) = \frac{e_y(s)}{s} \end{cases} \quad (21)$$

where x_a is the augmented state vector.

The open-loop dynamics including mismatched disturbance (Eq. (6)) is extended to

$$\begin{cases} \dot{x}_a = A_a x_a + B_a u + B_r r + \bar{\xi}(t) \\ y_a = C_a x_a \end{cases} \quad (22)$$

where corresponding matrices are as follows

$$\begin{cases} A_a = \begin{bmatrix} 0_{n \times n} & C_p \\ 0_{n_p \times n} & A_p \end{bmatrix}, B_a = \begin{bmatrix} D_p \\ B_p \end{bmatrix}, B_r = \begin{bmatrix} -I_{n \times n} \\ 0_{n_p \times n} \end{bmatrix}, C_a = [0_{n \times n}, C_p] \\ \bar{\xi}(t) = [0_{1 \times n}^T, \xi^T(t)]^T \end{cases} \quad (23)$$

Then the baseline control for the extended open-loop systems is written as

$$u_{bl} = -K_x x_a = -K_I e_{yI} - K_F x_p \quad (24)$$

where the controller parameters matrix is

$$K_x = [K_I, K_F] \quad (25)$$

The static gain matrix for controller indicates ease practical testing, validation, and possibly on-site re-tuning.⁵ In terms of tuning methods, Linear Quadric Regulation (LQR)

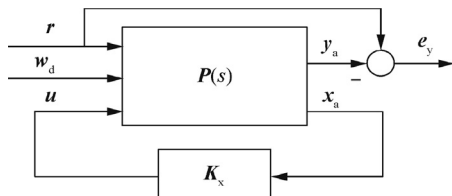


Fig. 8 General interconnection for H-infinity synthesis.

method^{13,23} is applied to tune the baseline controller gain K_x . Although the controller tuned by LQR method achieves ideal tracking performance for step-input commands, it ignores mismatched disturbance and input energy limitations. Therefore, a general H-infinity synthesis is adopted in Fig. 8, and $P(s)$ is integrated system model.

Then the considered controller parameter tuning is to solve the following optimization problem:

$$\min_{K_x} \max_{i=1,2,\dots,n_s} \|T_i(K_x)\|_{\infty} \text{ Subject to } K_x \text{ stabilizes } P(s) \text{ internally} \quad (26)$$

where $T_i(K_x)$ denotes that target function regarding specifications such as tracking accuracy, input energy limitations and disturbance attenuation. Since the H-infinity synthesis problem is no longer convex for structural constraints, we use the non-smooth approach²¹ to tune the proposed controller in Eq. (25).

In order to satisfy accurate command tracking with limited amplitude of control input, we address that

$$\begin{cases} T_1(K_x) = W_p T_{ry}(s) \\ T_2(K_x) = W_u T_{ru}(s) \end{cases} \quad (27)$$

where $T_{ry}(s)$ and $T_{ru}(s)$ respectively denote the closed-loop transfer function from reference command to system output and control input. H-infinity norm of closed transfer function $T_{ru}(s)$ is applied as the measurement of control energy. W_p and W_u are corresponding weighting functions.

Obviously, the parameters of weighting function make a great influence on the tuning results. Through selections of different weighting functions, closed-loop system bandwidth of each channel versus control energy is given in Fig. 9. Generally, the tracking bandwidth is conflicted with control input limitations under unit reference command, since high input energy is required to ensure a rapid response. Hence, we have to limit control energy by specifying an appropriate desired bandwidth in order to avoid large control effort that possibly leads to input saturation.

In addition to Eq. (27), another target function is addressed for disturbance rejection, which is written as

$$T_3 = W_d T_{dy}(s) \quad (28)$$

where $T_{dy}(s)$ denotes the closed-loop transfer function from mismatched disturbance to system output and W_d is weighting function.

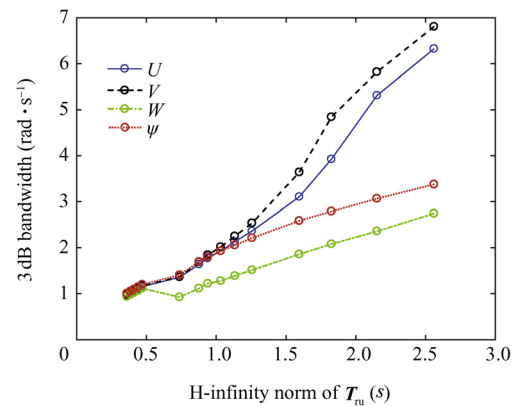


Fig. 9 Closed-loop system bandwidth of each channel versus $\|T_{ru}(s)\|_{\infty}$ (control energy).

Obviously, a small magnitude of $\|T_{dy}(s)\|$ is expected to attenuate mismatched disturbance. Therefore, the complete non-smooth H-infinity synthesis including Eqs. (27) and (28) are performed to ensure a good tradeoff among specifications on tracking, control effort limitation, and disturbance rejection.

After some repetitions, the selected weighting functions and the optimized gains are as follows

$$\left\{ \begin{array}{l} W_p = \text{diag}\left(\frac{0.65s+1}{0.0001s+1}, \frac{0.65s+1}{0.0001s+1}, \frac{0.65s+1}{0.0001s+1}, \frac{0.65s+1}{0.0001s+1}\right), W_u = \text{diag}\left(\frac{0.06s+1}{0.004}, \frac{0.06s+1}{0.004}, \frac{0.06s+1}{0.004}, \frac{0.06s+1}{0.004}\right) \\ W_d = \text{diag}\left(\frac{0.1s+1}{0.0002s+1}, \frac{0.1s+1}{0.0002s+1}, \frac{0.1s+1}{0.0002s+1}, \frac{0.1s+1}{0.0002s+1}\right), K_I = \begin{bmatrix} -2.1128 & -0.7185 & -0.5848 & -0.1829 \\ -1.5353 & 4.0945 & -0.2135 & 0.0548 \\ -4.1297 & -1.6229 & -0.2997 & 0.2429 \\ 0.1578 & 0.4557 & 0.3838 & 4.4664 \end{bmatrix} \\ K_F = \begin{bmatrix} -2.4965 & -0.7980 & -0.5150 & 0.0760 & 1.5327 & -0.1459 & -3.0408 & 9.5731 & -0.2056 \\ -1.7312 & 4.7419 & -0.2551 & 2.9849 & -0.2159 & 0.0029 & 16.8918 & 7.3047 & 0.0983 \\ -4.9066 & -1.8582 & -0.3198 & -0.1430 & 2.9646 & 0.2115 & -6.8105 & 19.0384 & 0.3371 \\ 0.2055 & 0.5535 & 0.5183 & 0.2262 & -0.3146 & 3.6882 & 1.6571 & -0.5796 & 5.6525 \end{bmatrix} \end{array} \right.$$

Fig. 10 shows that singular value plots of $T_{ry}(s)$, $T_{dy}(s)$ and $T_{ru}(s)$ that respectively demonstrates the archived tracking performance, the ability to disturbance rejection and the constrained control energy of the resulted closed-loop system. Therefore, the performance of closed-loop system is validated in frequency domain. The next step is the corresponding simulation in time domain.

3.2. Simulation of the novel ducted fan aircraft under mismatched disturbance

The disturbance $d(t)$ stands for external forces and moments, where the components are described by Dryden model.³² The disturbance is constructed by filtered Gaussian white noise $n(t)$ with zero mean

$$d(s) = G_f(s)n(s) \quad (29)$$

where $G_f(s)$ is a low-pass filter with bandwidth ω_f , and we have

$$G_f(s) = \frac{1}{s/\omega_f + 1} \quad (30)$$

The Power Spectral Density (PSD) of $n(t)$ is given as n_0 , then we have the approximated power of the filtered signal

$$P_n \approx \frac{n_0 \omega_f}{2} \quad (31)$$

Then the standard deviation of the filtered signal is

$$\sigma_n = \sqrt{P_n} \approx \sqrt{\frac{n_0 \omega_f}{2}} \quad (32)$$

In this work, we choose a low-pass filter with bandwidth at $\omega_f = 2.5$ rad/s and the standard deviation of each disturbance channel is 0.4, as shown in Fig. 11. To verify the effectiveness of the tuned controller, simulation results for the close-loop system under mismatched disturbance are plotted in Figs. 12 and 13.

Fig. 12 reveals that the closed-loop system achieves to track reference command in a rapid speed and small tracking error. Clearly the closed-loop system is able to maintain its command tracking abilities in the presence of mismatched disturbance.

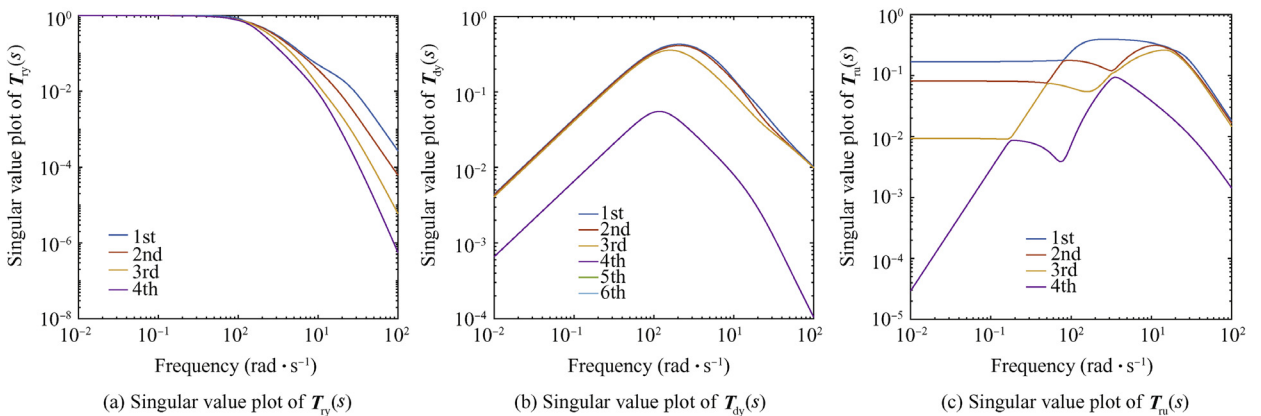


Fig. 10 Singular value plots of $T_{ry}(s)$, $T_{dy}(s)$ and $T_{ru}(s)$.

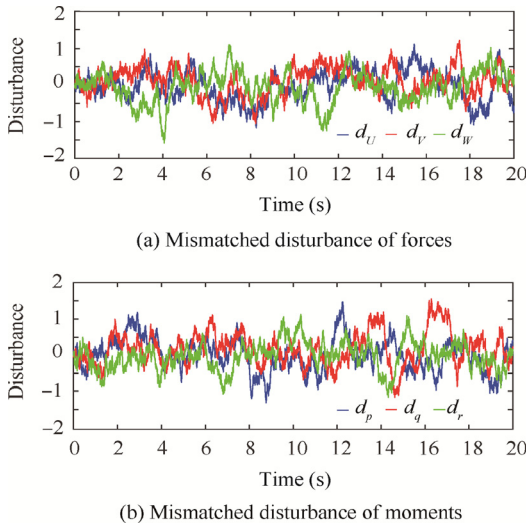


Fig. 11 Mismatched disturbance for simulation.

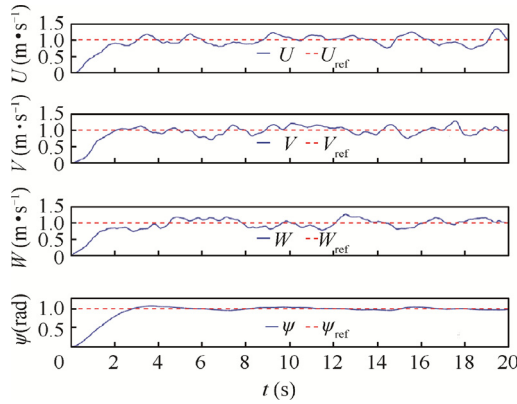


Fig. 12 System outputs of reference tracking response under mismatched disturbance.

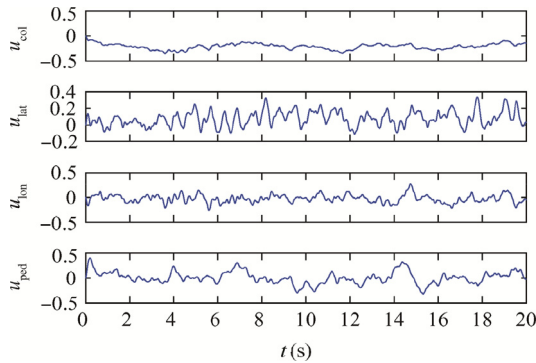


Fig. 13 Control inputs of reference tracking response under mismatched disturbance.

As plotted in Fig. 13, the amplitude of control inputs is constrained within $[-0.5, 0.5]$, since target function Eq. (27) for control energy limitation is applied. It is interesting that the largest control effort is the pedal input (u_{ped}) that primarily

produces yaw moment. Therefore, there is less margin in yaw direction to compensate disturbance than other channels.

4. Adaptive control design considering system uncertainty, actuator fault and input saturation

Although the baseline controller designed by robust H-infinity synthesis is able to achieve satisfactory performance in the presence of mismatched disturbance, the robust performance cannot be ensured under large system uncertainty and actuator fault.²² In addition, the proposed H-infinity synthesis neglects the occurrence of input saturation. In this section, as shown in Fig. 6, the adaptive augmentation of the baseline controller will be designed to recover the desired performance under system uncertainty, actuator fault and even when input saturation is active.

4.1. Adaptive control law with improved transient response and robustness

Similar to Eq. (22), the open-loop system with uncertainty and actuator fault is extended as

$$\dot{\mathbf{x}}_a = \mathbf{A}_a \mathbf{x}_a + \mathbf{B}_a \mathbf{A}(\mathbf{u} + \boldsymbol{\Theta}^T \boldsymbol{\Phi}(\mathbf{x}_p)) + \mathbf{B}_r \mathbf{r} \quad (33)$$

The state tracking error $\mathbf{e} = \mathbf{x}_a - \mathbf{x}_r$ is used to drive the composite adaptive control input

$$\mathbf{u} = \mathbf{u}_{\text{bl}} + \mathbf{u}_{\text{ad}} \quad (34)$$

where \mathbf{u}_{ad} is adaptive augmentation for the baseline control \mathbf{u}_{bl} .

Then we have the following equations with redefined regressive vector $\boldsymbol{\Phi}_a(\mathbf{u}_{\text{bl}}, \mathbf{x}_p)$

$$\begin{cases} \dot{\mathbf{x}}_a = \mathbf{A}_r \mathbf{x}_a + \mathbf{B}_a \mathbf{A}(\mathbf{u}_{\text{ad}} + \boldsymbol{\Theta}_a^T \boldsymbol{\Phi}_a(\mathbf{u}_{\text{bl}}, \mathbf{x}_p)) + \mathbf{B}_r \mathbf{r} \\ \boldsymbol{\Phi}_a(\mathbf{u}_{\text{bl}}, \mathbf{x}_p) = [\mathbf{u}_{\text{bl}}^T, \boldsymbol{\Phi}^T(\mathbf{x}_p)]^T \end{cases} \quad (35)$$

The extended uncertainty matrix is

$$\boldsymbol{\Theta}_a = [(\mathbf{I}_{n \times n} - \mathbf{A}^{-1})^T, \boldsymbol{\Theta}^T]^T \quad (36)$$

The reference dynamics to be followed is written as

$$\begin{cases} \dot{\mathbf{x}}_r = \mathbf{A}_r \mathbf{x}_r + \mathbf{B}_r \mathbf{r} \\ \mathbf{A}_r = \mathbf{A}_a - \mathbf{B}_a \mathbf{K}_e \end{cases} \quad (37)$$

Note that the reference model is the nominal closed-loop system stabilized by baseline controller. In order to improve the transient characteristics of the closed-loop dynamics, the observer-like reference model¹³ is written as

$$\dot{\mathbf{x}}_r = \mathbf{A}_r \mathbf{x}_r + \mathbf{B}_r \mathbf{r} + \mathbf{K}_e \mathbf{e} \quad (38)$$

where \mathbf{K}_e is the error feedback gain.

The adaptive control input is calculated by estimated uncertainty. $\hat{\boldsymbol{\Theta}}_a$ and $\boldsymbol{\Phi}_a(\mathbf{u}_{\text{bl}}, \mathbf{x}_p)$

$$\mathbf{u}_{\text{ad}} = -\hat{\boldsymbol{\Theta}}_a^T \boldsymbol{\Phi}_a(\mathbf{u}_{\text{bl}}, \mathbf{x}_p) \quad (39)$$

which is substituted to Eq. (35) to give

$$\begin{cases} \dot{\mathbf{x}}_a = \mathbf{A}_r \mathbf{x}_a - \mathbf{B}_a \mathbf{A} \Delta \boldsymbol{\Theta}_a^T \boldsymbol{\Phi}_a(\mathbf{u}_{\text{bl}}, \mathbf{x}_p) + \mathbf{B}_r \mathbf{r} \\ \Delta \boldsymbol{\Theta}_a = \hat{\boldsymbol{\Theta}}_a - \boldsymbol{\Theta}_a \end{cases} \quad (40)$$

Then the equation for tracking error is deduced as

$$\dot{\mathbf{e}} = (\mathbf{A}_r - \mathbf{K}_e) \mathbf{e} - \mathbf{B}_a \mathbf{A} \Delta \boldsymbol{\Theta}_a^T \boldsymbol{\Phi}_a(\mathbf{u}_{\text{bl}}, \mathbf{x}_p) \quad (41)$$

The error feedback gain is given as the following Algebraic Riccati Equation (ARE)²²

$$\begin{cases} PA_r^T + A_r P - PR^{-1}P + Q = 0 \\ Q = Q_0 + \left(\frac{\alpha+1}{\alpha}\right)I_{n \times n} \\ R = \frac{\alpha}{\alpha+1}I_{n \times n} \\ K_e = PR^{-1} \end{cases} \quad (42)$$

where Q_0 and α are tuning parameters.

The observer closed-loop matrix is

$$A_c = A_r - K_e = A_r - P\left(1 + \frac{1}{\alpha}\right) \quad (43)$$

Substitute it to Eq. (42), we have

$$\begin{cases} PA_c^T + A_c P = -PR^{-1}P - Q < 0 \\ A_c^T P^{-1} + P^{-1} A_c = -R^{-1} - P^{-1}QP^{-1} < 0 \end{cases} \quad (44)$$

The adaptive control laws with adaption rate Γ_a is selected as

$$\dot{\hat{\Theta}}_a = \Gamma_a \Phi_a(u_{bl}, x_p) e^T P^{-1} B_a \quad (45)$$

In order to perform stability analysis, we choose the Lyapunov function candidate

$$V(e, \Delta\Theta_a) = e^T P^{-1} e + \text{trace}(\Lambda \Delta\Theta_a^T \Gamma_a^{-1} \Delta\Theta_a) \quad (46)$$

Then we have

$$\begin{aligned} \dot{V}(e, \Delta\Theta_a) &= e^T P^{-1} \dot{e} + \dot{e}^T P^{-1} e + 2\text{trace}(\Lambda \Delta\Theta_a^T \Gamma_a^{-1} \dot{\hat{\Theta}}_a) \\ &= -e^T (R^{-1} + P^{-1}QP) e \\ &\quad + 2\text{trace}(\Lambda \Delta\Theta_a^T (\Gamma_a^{-1} \dot{\hat{\Theta}}_a - \Phi_a(u_{bl}, x_p) e^T P^{-1} B_a)) \\ &= -e^T (R^{-1} + P^{-1}QP) e \leq 0 \end{aligned} \quad (47)$$

Eq. (47) indicates that the state tracking error e is uniformly bounded in time. In addition, the second derivative of $V(e, \Delta\Theta_a)$ is written as

$$\ddot{V}(e, \Delta\Theta_a) = 2e^T (-R^{-1} - P^{-1}QP^{-1}) \dot{e} < 0 \quad (48)$$

Note the second time derivative of the Lyapunov function is also uniformly bounded, which yields that the system is globally asymptotically stable by Barbalat's lemma¹³ and the state tracking error satisfies $\lim_{t \rightarrow \infty} \|e(t)\| = 0$.

To perform transient dynamics analysis, Eq. (41) is rewritten as

$$\begin{cases} \dot{e} = (A_r - \frac{\alpha+1}{\alpha}P)e - \theta(t) \\ \theta(t) = B_a \Lambda \Delta\Theta_a^T \Phi_a(u_{bl}, x_p) \end{cases} \quad (49)$$

Then we have the asymptotic relation²² that defines the corresponding convergence rate

$$P = P_0 + O(\alpha), \text{ as } \alpha \rightarrow 0 \quad (50)$$

where O denotes Bachmann–Landau asymptotic order notation.³³

If we set a constant positive definite symmetric matrix P_0 , we can deduce

$$\dot{e} = \frac{1}{\alpha}(\alpha A_r - (\alpha+1)(P_0 + O(\alpha)))e - \theta(t) \quad (51)$$

The Eq. (51) can be viewed as singularly perturbed system, where α is a small parameter. In this case, we can claim that for a sufficiently small $\alpha > 0$, while starting from an initial time t_0 , this singular perturbation system has a unique solution $e(t, \alpha)$ on an infinite interval.²² Then we have the following conclusion about system state^{13,22}

$$x(t, \alpha) = \exp\left(-P_0\left(\frac{t-t_0}{\alpha}\right)\right)(x(t_0) - x_r(t_0)) + x_r(t) + O(\alpha)o(1) \quad (52)$$

where $o(1)$ is a function of time with $\lim_{t \rightarrow \infty} o(1) = 0$, and $O(1)$ decays to zero no slower than α .

Eq. (52) indicates that quantifiable transient characteristics of the closed-loop tracking performance can be ensured using sufficiently small parameter α , so as to reduce oscillations in the adaptive control system.¹²

Note that the proposed control law only considers matched uncertainty. Although the mismatched disturbance has been sufficiently discussed and rejected by the nominal baseline controller for the reference dynamics, we still need to make some modifications to achieve a more robust result. In this work, dead-zone modification and projection operator¹² are combined as the robustness modifications to Eq. (45)

$$\begin{cases} \dot{\hat{\Theta}}_a = \text{proj}\left(\hat{\Theta}_a, \Gamma_a \Phi_a(u_{bl}, x_p) \mu(\|e\|) e^T P^{-1} B_a\right) \\ \mu(\|e\|) = \max\left(0, \min\left(1, \frac{\|e\| - \gamma e_0}{(1-\gamma)e_0}\right)\right), \gamma \in (0, 1) \end{cases} \quad (53)$$

where $\mu(\|e\|)$ represents dead-zone modification, which prevents adaptive parameters from drifting away due to noise, system uncertainty and external disturbance.³¹ And $\text{proj}()$ denotes projection operator which is defined as

$$\begin{cases} \text{proj}(\beta, \Gamma x) = \begin{cases} x - \frac{\Gamma \nabla f(\beta)(\nabla f(\beta))^T x f(\beta)}{(\nabla f(\beta))^T \Gamma \nabla f(\beta)} & \text{if } f(\beta) > 0 \cap (x^T \nabla f(\beta)) > 0 \\ x & \text{if not} \end{cases} \\ f(\beta) = \frac{(1+\varepsilon)\|\beta\|^2 - \beta_{\max}^2}{\varepsilon \beta_{\max}^2} \quad |\beta| \leq \beta_{\max} \end{cases} \quad (54)$$

where β , Γ , and x are projection variables, ∇ denotes gradient operator, β_{\max} and ε are tuned parameters.

The adaptive control law modified by projection operator will force the tracking error to become small by preventing the adaptive parameters evolving out of the preset bounds. It also helps to avoid undesirable windup phenomenon for non-linear integrators.

4.2. Adaptive control law modification for input saturation

The ability to deal with input saturation is one of the fundamental problems for practical applications, especially along with disturbance and actuator fault. The saturation function is defined as

$$\text{sat}(x) = \begin{cases} x & |x| \leq b \\ b \text{sign}(x) & |x| > b \end{cases} \quad (55)$$

where b is the allowable bound of the saturated variable x . This saturation function is imposed on each component of control input, and the difference vector between designed input and the saturated input is calculated as

$$\Delta \mathbf{u} = [u_{\text{col}} - \text{sat}(u_{\text{col}}), u_{\text{lat}} - \text{sat}(u_{\text{lat}}), u_{\text{lon}} - \text{sat}(u_{\text{lon}}), u_{\text{ped}} - \text{sat}(u_{\text{ped}})]^T \quad (56)$$

In this work, motivated by dynamic anti-windup compensators,³⁴ the reference model is modified to adapt intensity of the saturation by reducing magnitude of reference signal during the transient process. In that case, the reference model (Eq. (38)) is evolved to

$$\dot{\mathbf{x}}_r = \mathbf{A}_r \mathbf{x}_r + \mathbf{B}_r (\mathbf{r} + \mathbf{K}_u \Delta \mathbf{u}) + \mathbf{K}_e \mathbf{e} \quad (57)$$

Similar to those steps in Section 4.1, we have the following error dynamics

$$\begin{cases} \dot{\mathbf{e}} = (\mathbf{A}_r - \mathbf{K}_e) \mathbf{e} - \mathbf{B}_a \mathbf{A} (\Delta \Theta_a^T \Phi_a(\mathbf{u}_{\text{bl}}, \mathbf{x}_p)) - \mathbf{B}_r \Delta \mathbf{K}_u \Delta \mathbf{u} \\ \Delta \mathbf{K}_u = \hat{\mathbf{K}}_u - \mathbf{K}_u \end{cases} \quad (58)$$

Choose the Lyapunov function candidate

$$\begin{aligned} V(\mathbf{e}, \Delta \Theta_a, \Delta \mathbf{K}_u) &= \mathbf{e}^T \mathbf{P}^{-1} \mathbf{e} + \text{trace}(\mathbf{A} \Delta \Theta_a^T \Gamma_a^{-1} \Delta \Theta_a) \\ &\quad + \text{trace}(\Delta \mathbf{K}_u^T \Gamma_u^{-1} \Delta \mathbf{K}_u) \end{aligned} \quad (59)$$

If we apply the modified adaptive control law for input saturation

$$\dot{\hat{\mathbf{K}}}_u = \Gamma_u \Delta \mathbf{u} \mathbf{e}^T \mathbf{P}^{-1} \mathbf{B}_a \quad (60)$$

where Γ_u is adaption rate for input saturation.

The time derivative of $V(\mathbf{e}, \Delta \Theta_a, \Delta \mathbf{K}_u)$ can be computed as

$$\begin{aligned} \dot{V}(\mathbf{e}, \Delta \Theta_a, \Delta \mathbf{K}_u) &= -\mathbf{e}^T (\mathbf{R}^{-1} + \mathbf{P}^{-1} \mathbf{Q} \mathbf{P}) \mathbf{e} \\ &\quad + 2 \text{trace}(\mathbf{A} \Delta \Theta_a^T (\Gamma_a^{-1} \dot{\Theta}_a - \Phi_a(\mathbf{u}_{\text{bl}}, \mathbf{x}_p) \mathbf{e}^T \mathbf{P}^{-1} \mathbf{B}_a)) \\ &\quad + 2 \text{trace}(\Delta \mathbf{K}_u^T (\Gamma_u^{-1} \dot{\hat{\mathbf{K}}}_u - \Delta \mathbf{u} \mathbf{e}^T \mathbf{P}^{-1} \mathbf{B}_a)) \\ &= -\mathbf{e}^T (\mathbf{R}^{-1} + \mathbf{P}^{-1} \mathbf{Q} \mathbf{P}) \mathbf{e} \leq 0 \end{aligned} \quad (61)$$

Therefore, global asymptotic tracking is proved for the proposed system in the presence of input saturations. In particular, we also use projection operator to limit adaptive gain \mathbf{K}_u to avoid integrator windup problems, which is represented by

$$\dot{\hat{\mathbf{K}}}_u = \text{proj}(\hat{\mathbf{K}}_u, \Gamma_u \Delta \mathbf{u} \mathbf{e}^T \mathbf{P}^{-1} \mathbf{B}_a) \quad (62)$$

Due to feedback term $\mathbf{K}_u \Delta \mathbf{u}$ that is attached to the proposed reference model, the reference command is reduced to compensate saturations, as the cost of delayed transient response.

4.3. Numerical simulation of the novel ducted fan aircraft

In previous sections, rigorous design steps for robust adaptive control have been detailed. In order to evaluate the

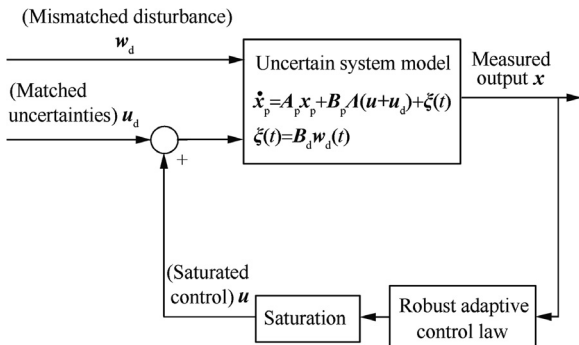


Fig. 14 Evaluation model of the novel ducted fan aircraft.

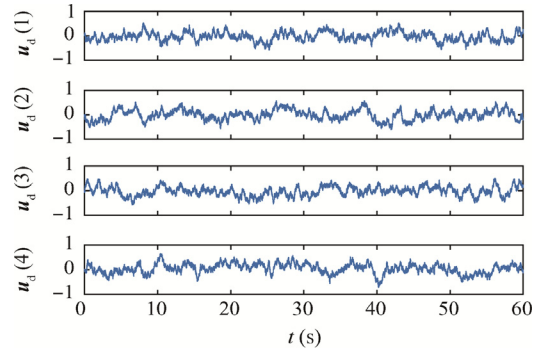


Fig. 15 Matched system uncertainty for simulation of novel ducted fan aircraft.

effectiveness of the proposed algorithm, a series of simulations are performed on our novel ducted fan aircraft. System parameters are taken from the results in Section 2.1. In the simulation, evaluation model includes system uncertainty, mismatched disturbance and actuator fault, as shown in Fig. 14. The uncertain system is written as

$$\begin{cases} \dot{\mathbf{x}}_p = \mathbf{A}_p \mathbf{x}_p + \mathbf{B}_p \mathbf{A}(\mathbf{u} + \mathbf{u}_d) + \boldsymbol{\xi}(t) \\ \boldsymbol{\xi}(t) = \mathbf{B}_d \mathbf{w}_d(t) \end{cases} \quad (63)$$

In terms of mismatched disturbance, we adopt the same signal (see Fig. 11) in Section 3.2. \mathbf{A} is set to 0.75 to account for 25% loss of effectiveness that regards to actuator fault. The matched system uncertainty is denoted by \mathbf{u}_d , which is also approximated by filtered Gaussian white noise (Eq. (29)) and given in Fig. 15. The corresponding parameters of \mathbf{u}_d is

$$\begin{cases} \omega_f(\mathbf{u}_d) = 1.5 \text{ rad/s} \\ \sigma(\mathbf{u}_d) \approx 0.2 \end{cases}$$

where $\omega_f(\cdot)$ and $\sigma(\cdot)$ respectively denotes standard deviation and bandwidth.

In our adaptive control law, the term $\Theta^T \Phi(\mathbf{x}_p)$ is used to estimate the system uncertainty \mathbf{u}_d , and as for simplicity, we adopt the following regressive function

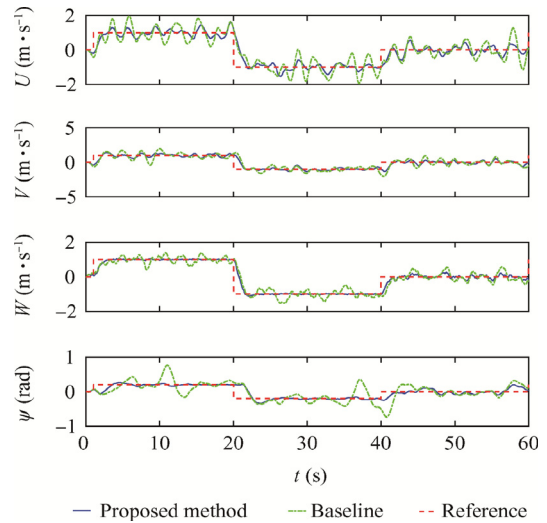


Fig. 16 System outputs of reference tracking response by baseline control and adaptive control (no input saturation).

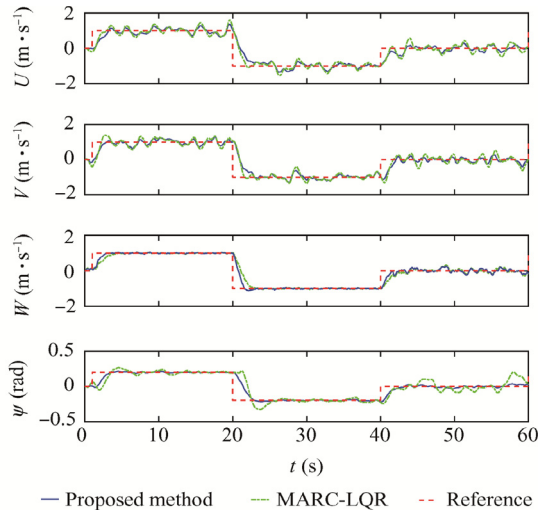


Fig. 17 System outputs of reference tracking response by proposed method and MARC-LQR method (no input saturation).

$$\Phi(x_p) = x_p \quad (64)$$

The other parameters of adaptive control law are given as

$$\mathbf{Q}_0 = 80\mathbf{I}_{13 \times 13}, \quad \alpha = 0.1, \quad \mathbf{\Gamma}_a = 5\mathbf{I}_{13 \times 13}, \quad \mathbf{\Gamma}_u = -2.9\mathbf{I}_{4 \times 4}$$

And the maximum allowable bound for the projection operator is set to 2.

In the first simulation, we will validate the performance of the proposed adaptive method with no input saturation. Fig. 16 provides reference tracking response of the ducted fan aircraft by baseline control and adaptive control. Section 3.2 shows that the baseline controller enables nominal system to achieve satisfied performance. However, when matched uncertainty and actuator fault is included, the robust baseline controller alone reveals large tracking error, whereas the adaptive controller keeps good performance. Therefore, the advantage of the adaptive augmentation over the baseline controller is verified.

In terms of baseline control tuning, (LQR)^{13,22,23} method has been applied by classic MRAC method. It is pointed out that one short of LQR method is the ignorance of mismatched disturbance, which has been considered by our algorithm. Reference tracking response conducted by the proposed method and its comparison are plotted in Fig. 17. Compared to classic MRAC-LQR algorithm, the proposed method enables a faster tracking speed and smaller fluctuation, especially for yaw channel. This progress of system performance is attributed to the adoption of H-infinity synthesis for baseline control, and observer-like reference model for its adaptive augmentation. The reason for the existence of tracking error is that the closed-loop system is under continuous matched uncertainty and mismatched disturbance at very large magnitude (see Figs. 11 and 15). In addition, the control effort to attenuate these uncertainty and disturbance and the bandwidth of actuators are limited. Therefore, the tracking error cannot be extremely small.

In the next simulation, we will test performance of closed-loop system with the activated actuator saturation. The allowable bound of control input is 0.5 for each control channel, which is very serious saturation. The corresponding reference tracking response and control input are respectively

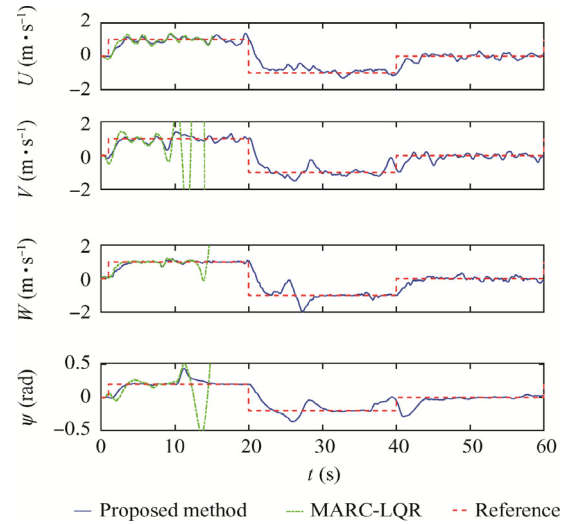


Fig. 18 System outputs of reference tracking response by the proposed method and MARC-LQR method (with input saturation).

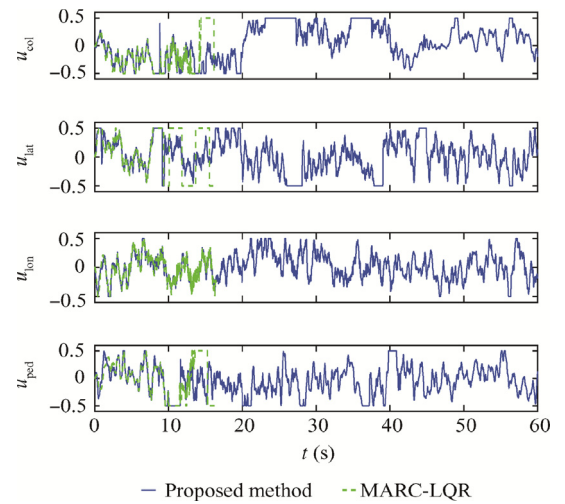


Fig. 19 Control input of reference tracking response by proposed method and MARC-LQR method (with input saturation).

plotted in Figs. 18 and 19. We can observe that the classic MRAC-LQR controller fails to maintain stability, while the proposed method still provides satisfied response in the transient phase. Note that tracking performance is unavoidable degraded, because in the proposed reference model (Eq. (57)), the reference command is reduced to compensate the saturated control input, indicating that system response is delayed.

5. Conclusions

This study presents a robust adaptive control of novel tandem coaxial ducted fan aircraft. The comprehensive controllability analysis provides a detailed assessment of the controllability of the prototype as well as the margin to reject mismatched disturbance. In this way, the primary challenge for the flight control design is attributed to poor controllability in roll direction,

and low margin for disturbance rejection in yaw direction. Based on the control-oriented model, a control framework combining robust baseline controller and its adaptive augmentation is proposed. Mismatched disturbance attenuation is ensured by the robust baseline controller tuned by H-infinity synthesis. To deal with system uncertainty, actuator fault and input saturation, the adaptive augmentation of the baseline control is applied. In order to illustrate the superiority of the proposed method, we compare our results with those classic MRAC methods^{13,22,23} by numerical simulation. The simulation results showed that, for system uncertainty, mismatched disturbance and actuator fault, the proposed algorithm achieves the closed-loop system better transient response and more robust margin than the classic MRAC method. Especially when input saturation is activated, the proposed method provides slightly degraded performance whereas the classic MARC method deteriorates to be instable.

There is still certain margin to improve the proposed method in near future. For instance, systematic methodology to select parameters (Q_0 , α , Γ_a , and Γ_u) for the adaptive control can be researched to achieve better system performance. In addition, simulation on nonlinear model or real flights should be performed to further validate the proposed algorithms. Another possible research topic could be robust control considering time delay or bandwidth limitation of actuators.

References

1. Ko A, Ohanian O, Gelhausen P. Ducted fan UAV modeling and simulation in preliminary design. *AIAA modeling and simulation technologies conference and exhibit*; 2007 Aug 20–23; Hilton Head. Reston: AIAA; 2007. p. 1–10.
2. Wang Z, Liu Z, Fan N, Guo M. Flight dynamics modeling of a small ducted fan aerial vehicle based on parameter identification. *Chin J Aeronaut* 2013;**26**(6):1439–48.
3. Naldi R, Gentili L, Marconi L, Sala A. Design and experimental validation of a nonlinear control law for a ducted-fan miniature aerial vehicle. *Control Eng Pract* 2010;**18**(7):747–60.
4. Xu B, Wang X, Xiang C, Ma Y. Modelling and hovering control of a novel multi-tandem ducted fan vehicle. *2015 International conference on unmanned aircraft systems (ICUAS)*; 2015 June 9–12; Denver. Piscataway: IEEE Press; 2015. p. 1346–54.
5. Xiang C, Wang Y, Ma Y, Xu B. Robust flight control using nonsmooth optimization for a tandem ducted fan vehicle. *Asian J Control* 2016;**18**(5):1805–24.
6. Sheng S, Sun C. A near-hover adaptive attitude control strategy of a ducted fan micro aerial vehicle with actuator dynamics. *Appl Sci* 2015;**5**(4):666–8.
7. Hess RA, Bakhtiari-Nejad M. Sliding-mode control applied of a nonlinear model of an unmanned aerial vehicle. *J Guidance, Control, Dynam* 2008;**31**(4):1163–6.
8. Aruneshwaran R, Suresh S, Wang J, Venugopalan, TK. Neural adaptive flight controller for ducted-fan UAV performing nonlinear maneuver. *Computational intelligence for security and defense applications (CISDA)*; 2013 Apr 16–19; Singapore. Piscataway: IEEE Press; 2013. p. 51–6.
9. He W, Ouyang Y, Hong J. Vibration control of a flexible robotic manipulator in the presence of input deadzone. *IEEE Trans Ind Inf* 2016;**13**(1):48–59.
10. He W, Chen Y, Yin Z. Adaptive neural network control of an uncertain robot with full-state constraints. *IEEE Trans Cybern* 2016;**46**(3):620–9.
11. He W, Dong Y. Adaptive fuzzy neural network control for a constrained robot using impedance learning. *IEEE Trans Neural Networks Learn Syst* 2017; PP(99):1–13.
12. Sheng S, Sun C, Zhao H. Indirect adaptive attitude control for a ducted fan vertical takeoff and landing microaerial vehicle. *Mathe Probl Eng* 2015;**6**:1–13.
13. Valavanis KP, Vachtsevanos GJ. *Handbook of unmanned aerial vehicles: A springer live reference*. Berlin: Springer-Verlag; 2011. p. 1125–230.
14. Hu T, Lin Z. *Control systems with actuator saturation: analysis and design*. Berlin: Springer Science & Business Media; 2001. p. 327–30.
15. Guilhem P, Jean-Marc B. Application of robust antiwindup design to the longitudinal aircraft control to cover actuator loss. *IFAC Proc Vol* 2013;**46**(19):506–11.
16. Chen M, Wu Q, Jiang C, Jiang, B. Guaranteed transient performance based control with input saturation for near space vehicles. *Sci China Inf Sci* 2014;**57**(5):1–12.
17. He W, He X, Ge S. Vibration control of flexible marine riser systems with input saturation. *IEEE/ASME Trans Mechatron* 2016;**21**(1):254–65.
18. He W, Dong Y, Sun C. Adaptive neural impedance control of a robotic manipulator with input saturation. *IEEE Trans Syst, Man, Cybernet: Syst* 2016;**46**(3):334–44.
19. Zhang L, Xie W, Wang J. Robust MPC for linear systems with structured time-varying uncertainties and saturating actuator. *Asian J Control* 2017;**19**(3):1197–204.
20. Skogestad S, Postlethwaite I. *Multivariable feedback control: Analysis and design*. New York: Wiley; 2007. p. 100–5.
21. Gahinet P, Apkarian P. Structured H-infinity synthesis using MATLAB. *18th IFAC world congress*; 2011 Aug 28–September 2; Milano. Laxenburg: IFAC; 2011. p. 1435–40.
22. Eugene L, Kevin W. *Robust and adaptive control with aerospace applications*. Berlin Heidelberg: Springer; 2013. p. 175–80.
23. Wiese D, Annaswamy A, Muse J, Bolender M, Lavretsky E. Adaptive output feedback based on closed-loop reference models for hypersonic vehicles. *J Guid, Control Dyn* 2015;**38**(12):2429–40.
24. Hussain H, Annaswamy A, Lavretsky E. A new approach to robust adaptive control. *American control conference (ACC)*; 2016 Jul 6–8; Boston. Piscataway: IEEE Press; 2016. p. 3856–61.
25. Johnson EN, Turbe MA. Modeling, control, and flight testing of a small ducted fan aircraft. *J Guid, Control Dyn* 2006;**29**(4):769–79.
26. Zhang Y, Xiang C, Xu B, Fan W. Comprehensive nonlinear modeling and attitude control of a novel tandem ducted fan vehicle. *IEEE international conference on aircraft utility systems (AUS)*; 2016 October 10–12; Beijing. Piscataway: IEEE Press; 2015. p. 50–6.
27. Jang I, Jeong J, Shin H, Kim S, Tsourdos A, Suk J. Cooperative control for a flight array of UAVs and an application in radar jamming. *IFAC-Papers On Line* 2017;**50**(1):8011–8.
28. Cai G, Chen B, Lee T, Lum K. Comprehensive nonlinear modeling of an unmanned-aerial-vehicle helicopter. *AIAA guidance, navigation and control conference and exhibit*; 2008 August 18–21; Honolulu. Reston: AIAA; 2008. p. 7414–38.
29. Tischler M, Remple R. *Aircraft and rotorcraft system identification*. Reston: AIAA; 2006. p. 95–110.
30. Chen Y, Atherton D. *Linear feedback control: analysis and design with MATLAB*. Philadelphia: SIAM; 2007. p. 120–5.
31. Zhou K, Doyle JC. *Essentials of robust control*. Upper Saddle River: Prentice hall; 1998. p. 155–60.
32. Decker, Barbré J. Temporal wind pairs for space launch vehicle capability assessment and risk mitigation. *J Spacecraft Rockets* 2014; **52**(1):209–16.
33. Kevorkian J, Cole J. *Multiple scale and singular perturbation methods*. Berlin Heidelberg: Springer Science & Business Media; 2012. p. 127–30.
34. Sarhadi P, Noei AR, Khosravi A. Adaptive μ -modification control for a nonlinear autonomous underwater vehicle in the presence of actuator saturation. *Int J Dynam Control* 2017;**5**(3):596–603.